Graphical Abstract

Comprehensive correlation for the prediction of the heat transfer through a single droplet in dropwise condensation regime

Jérémie Lethuillier, Marc Miscevic, Pascal Lavieille, Stéphane Blanco, Christophe Coustet, Frédéric Topin

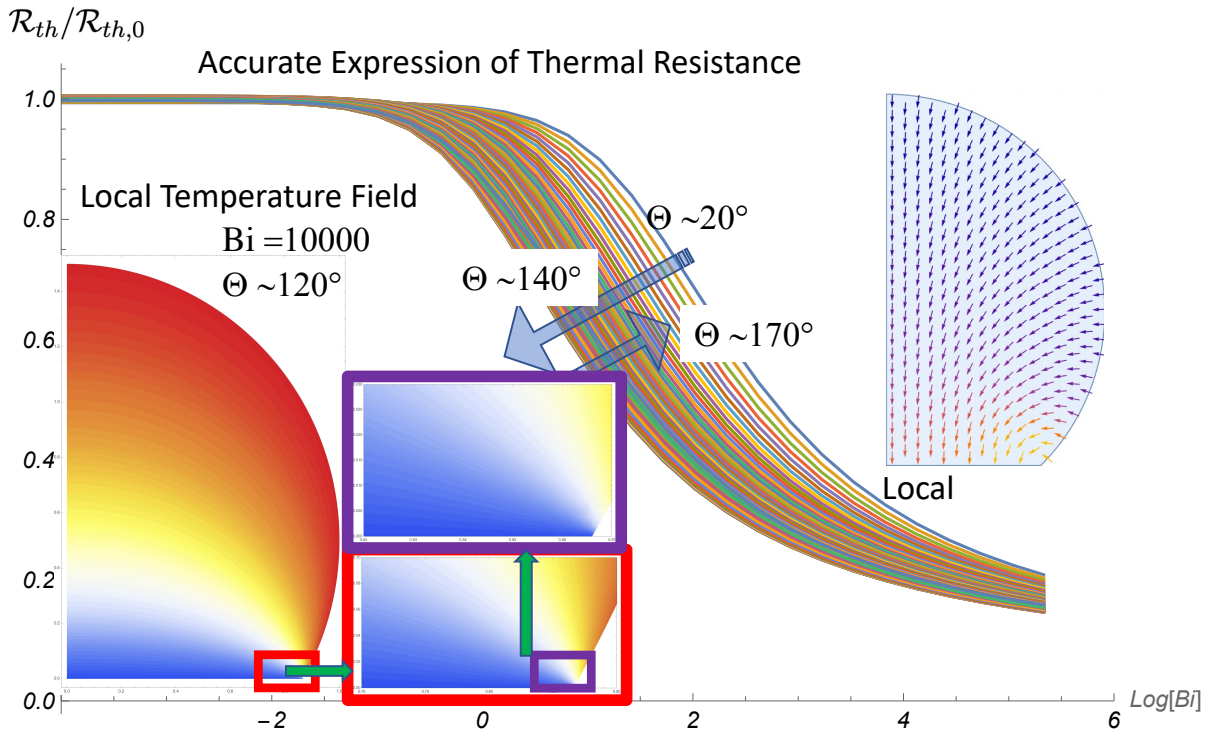

Highlights

Comprehensive correlation for the prediction of the heat transfer through a single droplet in dropwise condensation regime

Jérémie Lethuillier, Marc Miscevic, Pascal Lavieille, Stéphane Blanco, Christophe Coustet, Frédéric Topin

- Available laws lead to huge discrepancies when they are compared to each other;
- Elements of the mesh must be smaller than the inverse of the local Biot number;
- An unbiased correlation is provided to calculate the conduction thermal resistance;
- In dropwise condensation this law is valid whatever the Biot number and contact angle.

Comprehensive correlation for the prediction of the heat transfer through a single droplet in dropwise condensation regime

Jérémie Lethuillier[a], Marc Miscevic[a], Pascal Lavieille[a], Stéphane Blanco[a], Christophe Coustet[b], Frédéric Topin[a,c]

[a]LAPLACE, UMR CNRS-INP-UPS 5213, University of Toulouse, France
[b]MESOSTAR, France
[c]Aix Marseille Université, CNRS IUSTI, Marseille, France

Abstract

Numerical simulations have been performed to determine the conduction heat transfer in a sessile droplet for a large range of dynamic contact angle θ and Biot number Bi. The substrate is set at a constant and uniform temperature, while a convective heat transfer is set at the liquid-vapor interface. In such a configuration, the heat flux is concentrated in the triple line region, so that numerical results can become inaccurate as the Biot number increases. A reference case in which the heat flux can be determined analytically has thus be established to derive an empirical criterion on the local mesh refining needed to obtain accurate numerical results. To consolidate the results obtained with a finite elements code, calculations have been performed with a completely independent tool using Monte Carlo method on a set of cases. A correlation has then been derived from the numerical results data with a maximum deviation of less than 4% in the considered range of θ and Bi, that covers conditions encountered in all the studies dealing with dropwise condensation of pure vapor. Comparisons with other laws available in literature have then been performed, evidencing some important discrepancies.

Keywords: Heat transfer, thermal resistance, sessile drop, numerical simulation, correlation, dropwise condensation

1. Introduction

1.1. General considerations about the modeling of dropwise condensation

Condensation is commonly encountered in many situations both in nature (cloud, mist,...) or applications (heat exchangers, HVAC, ...) and could occurs either on cold surface or directly in gas phases. Two regimes are distinguished on surface condensation. The first one is filmwise condensation ; in that regime, the condensates form a continuous film that covers the cold substrate. In the second regime, i.e. dropwise regime, the condensates form small droplets separated from each other. The latter regime can appear in some portions of space and/or time, but is often reported in literature as difficult to maintain on an extended surface during long time. Droplet condensation is commonly reported in 2 situations (see. e.g. [1]): the direct contact condensation, and the dropwise condensation, first analyzed by Schmidt et al. [2], usually observed when vapor condensates on a hydrophobic surface. As dropwise condensation

is a very efficient condensation regime -compared to filmwise one- from heat transfer point of view it has generated a lot of scientific and industrial interest (see e.g. [3, 4, 5, 6]) ; yet the different processes composing dropwise condensation, involving the nucleation, the growth of a single droplet and its coalescence with the neighboring droplets are still not fully understood. Indeed, heat transfer coefficients up to few hundreds of thousands of $W.m^{-2}.K^{-1}$ are often reported in literature as discussed in Lethuillier et al. [7] for example. The main explanation for such a high value of the heat transfer coefficient is related to the very low characteristic dimensions of the droplets present on the substrate, leading to small values of the thermal resistances of each of these droplets. To predict the heat transfer rate, it is thus mandatory to determine the drop-size distribution, as well as the heat flux through each droplet belonging to a given size class.

Since the seventies, two approaches have been developed to predict the drop-size distribution. The first one based on population balance theory was initially developed by Wen and Jer [8]. They proposed to relate the cardinal of a given droplet size class to the number of droplets entering and exiting this class because of their growth, as well as the number of droplets disappearing from the class due to the sweeping of the substrate by the biggest droplets.

The resulting differential balance equation is then:

$$\frac{d(G(R)n(R))}{dR} + \frac{n(R)}{\tau} = 0 \tag{1}$$

where R is the curvature radius, $G(R) = \frac{dR}{dt}$ is the growth rate, $n(R)$ is the drop-size distribution and τ is the renewal characteristic time defined as the ratio between the sweeping rate and the substrate area. The growth rate $G(R)$ can be expressed from a simple energy balance, assuming quasi-static process, as:

$$G(R) = \frac{Q_d}{\rho_l \mathrm{L}_{lv} \pi R^2 (2 - 3\cos\theta + \cos^3\theta)} \tag{2}$$

The heat rate Q_d is evaluated from a heat transfer model through a single drop, as discussed in details in the following.

The second approach that have been developed to determine the drop-size distribution consists in following each drop during its lifecycle and is usually named "Individual Based Modelling". Due to the number of drops to be tracked, strong assumptions must be made to ensure acceptable computation times. In particular, all processes are generally considered quasi-statics and the drop birth as well as the coalescence events are supposed instantaneous. Although these strong assumptions, the implementation of individual based modelling has been demonstrated many times to be in good agreement with size distribution data available in literature regarding drop radii greater than few microns (see e.g. [7, 9, 10]). Unfortunately, as no reference data exist for the size distribution of the smaller drops, the distribution obtained with such an individual based model (as well as the one obtained with population balance approach) has not yet been validated. Moreover, it must be highlighted that the size distributions of small drops obtained respectively with individual-based and population-based models can be very different. This point has been emphasized in a previous work [7], showing that discrepancies up to two orders of magnitude can be obtained in the drop-size distribution value according to the used approach.

Whatever the model of the drop-size distribution, the heat rate through a single droplet must be expressed according to the various parameters of the considered configuration. One can cite

the wettability of the substrate, the wall subcooling, the physical properties of the working fluid, the interfacial heat transfer coefficient, etc. A short review of the main works related to the prediction of the thermal resistance of a sessile droplet is briefly summarized in the following section.

1.2. Droplet thermal resistance

For pure vapor, as considered in the following, Le Fevre and Rose [11] were the first to propose to breakdown the temperature jump between saturated vapor at T_{sat} and substrate's wall at T_w into 4 different terms corresponding respectively to:

- the temperature jump due to the heat conduction through the coating, at the surface of the solid substrate;
- the temperature jump due to the heat conduction through the liquid within the drop;
- the temperature jump due to the liquid-vapor interfacial thermal resistance;
- the temperature jump due to the effect of the curvature on the saturation conditions.

The imposed temperature difference $T_{sat} - T_w$ can then be expressed as:

$$T_{sat} - T_w = Q_d \times \frac{R_{th,coat} + R_{th} + R_{th,i}}{1 - \frac{R_{min}}{R}} \tag{3}$$

where the denominator $(1 - \frac{R_{min}}{R})$ corresponds to the effect of the curvature on the modification of the saturation conditions.
Commonly used expressions of thermal resistances $R_{th,coat}$, R_{th} and $R_{th,i}$ can be found in [7]. The expression of the effect of the coating appears to be quite reliable and is usually expressed as :

$$R_{th,coat} = \frac{\delta_{coat}}{\mathrm{k}_{coat}\pi R^2 sin^2\theta} \tag{4}$$

with δ_{coat} the thickness of the coating, k_{coat} the thermal conductivity and θ the dynamic contact angle.
On the other hand, there still exists an uncertainty on the evaluation of the interfacial thermal resistance. This latter is generally expressed as :

$$R_{th,i} = \frac{1}{2\pi R^2 h_i (1 - cos\theta)} \tag{5}$$

With h_i the heat transfer coefficient at the liquid-vapor interface, deduced from the kinetic model of Schrage [12] and reported in [13] as :

$$h_i = \frac{2f}{2 - f} \frac{1}{\sqrt{2\pi R_v T_{sat}}} \frac{\rho_v h_{lv}^2}{T_{sat}} (1 - \frac{P_{sat}}{2\rho_v h_{lv}}) \tag{6}$$

where h_{lv} is the latent heat of vaporisation, R_v is the mass ideal gas constant of the vapor, ρ_v is the vapor density and f is the condensation coefficient. This latter corresponds to the ratio between the rate of molecules that cross the liquid-vapor interface and the total rate

of molecules that hit the interface. This relation is often reported in dropwise condensation literature without the term $\frac{p_{sat}}{2\rho_v L_{lv}}$ [14, 15], which is quite reasonable for saturation pressure equal or less than normal atmospheric pressure. It should be noticed that in this expression, the condensation coefficient f is poorly documented. An important work remains thus to be done on the accurate prediction of this coefficient as a function of the various parameters (pressure, concentration of non-condensable gas, etc.) [7, 13].
Regarding the thermal resistance of the liquid within the drop (whose accurate prediction is the main goal of the present work), one of the most widely used expression is the one derived by Kim and Kim [16]. To establish this expression, the authors considered hydrophobic coatings, and postulated that each isotherm within the droplet is a sphere segment passing by the triple line. They then expressed the maximum distance between two consecutive isotherms and assumed that the average distance between two isotherms is half of this maximum distance. Finally by integrating the expression of the temperature difference between liquid-vapor interface and substrate's wall, they proposed the following thermal resistance due to heat conduction through the drop:

$$R_{th} = \frac{\theta}{4\pi R k_l \sin\theta} \tag{7}$$

Where k_l is the thermal conductivity of the liquid.

It must be noticed that this expression aims to predict the conduction thermal resistance when two Dirichlet boundary conditions are imposed, respectively at the foot of the drop and at the interface. This assumption is justified for the extreme contrast cases : i) when the interfacial heat transfer coefficient is infinite ($R_{th,i} << R_{th}$) and ii) when the interfacial transfer becomes so limiting that the drop becomes fairly isothermal at the wall temperature ($R_{th,i} >> R_{th}$).
In order to take into account the variation of R_{th} with the Biot number, Chavan et al. [14] numerically simulated the conduction heat transfer through a single droplet on an hydrophobic or superhydrophobic substrate with a convective exchange between interface and vapor and a prescribed temperature on the substrate. They used COMSOL finite element software to solve the 2-D axisymmetric case. Using the calculated temperature field and heat transfer rate across the drop they derived a droplet Nusselt number correlation by fitting the numerical results. From this expression, it can be deduced that the thermal resistance due to conduction in the droplet is expressed as, for dynamic contact angles θ in the range [90°;170°]:

$$R_{th} = \frac{1}{k_l R \sin\theta Nu} - \frac{1}{h_i\, 2\pi R^2 (1-\cos\theta)} \tag{8}$$

with:

$$Nu = 3\,\theta^{0.65}\,(Bi\sin\theta)^{0.83} + 0.007\,\theta^{5.1}\,(Bi\sin\theta)^{-0.23} \qquad \text{if } Bi\sin\theta < 0.5 \tag{9}$$

$$Nu = 0.29\,\theta^{2.24}\,(Bi\sin\theta)^{-0.17} + 3.33\,\theta^{-0.3}\,(Bi\sin\theta)^{0.72} \qquad \text{if } 0.5 < Bi\sin\theta \leq 2 \tag{10}$$

$$Nu = 5.76\ \mathrm{e}^{-0.28\,\theta^{0.68}} \ln(1 + 5\,(Bi\sin\theta)^{0.82} - 2.79\,(Bi\sin\theta)^{0.83}) \qquad \text{if } 2 < Bi\sin\theta \leq 10^5 \tag{11}$$

where Bi is the Biot number defined as $Bi = \frac{h_i R}{k_l}$.
Another recent and widely used expression for the conduction thermal resistance within a sessile droplet is the one proposed by Adhikari et al. [15] that aims to extend the validity range -compared to Chavan et al. correlation - to hydrophilic configurations. They also used

a numerical approach to determine the temperature field inside a droplet along with the heat transfer rate crossing it for a wide range of Biot number ($10^{-4} \leq \ Bi \ \leq 10^3$) and contact angle ($10° \leq \theta \leq 170°$) using the ANSYS thermal module. They then derived a correlation between Bi, the dynamic contact angle θ and the global thermal resistance $R_{th,g}$, this latter being the sum of the resistance due to the conduction in the liquid and the interfacial resistance. The expression of R_{th} that can be deduced from their global thermal resistance is then, for θ in the range $50° \leq \theta \leq 130°$ and $10^{-4} < Bi < 10^3$:

$$R_{th} = \frac{1}{\pi R^2 \sin^2\theta}\left(\frac{f(Bi,\theta)R}{k_l} + \frac{1}{2h_i}\right) - \frac{1}{h_i\, 2\pi R^2(1-\cos\theta)} \tag{12}$$

with

$$f(Bi,\theta) = 0.2160 + \frac{0.7278}{Bi} + \left(0.001465 - \frac{0.008086}{Bi}\right) \times \theta - 0.1012 \times \log_{10}(Bi) \\ - 0.01378 \times \log_{10}^2(Bi) + 0.007361 \times \log_{10}^3(Bi) \tag{13}$$

With a such a definition, the scaling factor $f(Bi,\theta)$ can become negative for small values of the Biot number in hydrophobic configuration.
Several remarks can be made regarding this correlation:

- At atmospheric pressure, the value of the interfacial heat transfer coefficient is often reported to be $15.7\,10^6\,W.m^{-2}.K^{-1}$. In this case, a Biot number of 1000 corresponds to a curvature radius of about $100\,\mu m$. The correlation proposed by Adhikari et al. can then not be used with confidence for droplets with curvature radius higher than 100 μm;

- For high value of the Biot number, the heat flux is concentrated on the triple line region. The convergence of the grid is then difficult to reach. This point will be discussed in details in the following.

1.3. Summary and main aims of the present work

So, whatever the approach (individual-based model or population balance model) used to predict the global heat transfer during dropwise condensation process, the conduction thermal resistance within the liquid of a single drop must be accurately predicted. Generally, one of the three most often used correlations available in literature is chosen, i.e., the one of Kim and Kim [16], Chavan et al. [14] or Adhikari et al. [15]. However, as it will be illustrated in the following, important discrepancies exist between the results given by these three correlations according to the configuration considered. Moreover, none of these correlations can be used alone with confidence for contact angle ranging from superhydrophilic to superhydrophobic situations, nor with Biot number varying over the full range encountered during dropwise condensation regime i.e. [10^{-4} , 10^5].
Thus, the main objective of this work is to provide a robust expression for the conduction thermal resistance R_{th} that can be used with confidence for all the conditions encountered in dropwise condensation. For that purpose, numerical simulations of heat transfer in a single droplet have been done for dynamic contact angle varying from 20° to 170° and Biot number varying from 10^{-4} to 10^5. A particular attention has been paid to the numerical precision, by comparing the results to both an analytical reference case and to the results given by a

dedicated numerical tool based on Monte Carlo method. Based on this analysis, an empirical criterion on the local mesh size has been established to ensure a good precision of the numerical results.

2. Physical model and numerical considerations

In order to calculate the thermal resistance by conduction through the liquid within a single drop, a simple quasi-static thermal model has been numerically set. The physical model that has been used, and described hereafter, is widely used in literature, as for instance in the work by Chavan et al [14] or Adhikari et al. [15]. Our study covers the combined domains of validity of these previous studies in terms of Biot and dynamic contact angle. We used basically the same set of assumptions (recalled below) considering heat transfer than in these previous works, so we will not repeat here the justifications of such assumptions.
The drop is 2D-axisymmetric in the (r,z) plane. In steady state, considering pure conduction heat transfer across the drop the energy equation reduces to Laplace equation:

$$\frac{\partial^2 T}{\partial z^2} + \frac{1}{r}\frac{\partial T}{\partial r} + \frac{\partial^2 T}{\partial r^2} = 0 \tag{14}$$

A constant and uniform temperature is imposed at the foot of the drop, while a convective heat transfer is imposed between the liquid-vapor interface and the vapor at T_∞. This heat transfer coefficient corresponds to the interfacial heat transfer coefficient h_i appearing in the interface thermal resistance $R_{th,i} = \frac{1}{h_i S_i}$. It is evaluated using Equation 6. As already mentioned in the *Introduction*, accurate prediction of h_i remains challenging as it is a function of the condensation coefficient which may vary by several orders of magnitude according to the experimental configuration (in particular according to the pressure and the non-condensable gas fraction). So, a huge range of variation will be considered in the following to cover as much as possible all possible cases.
The boundary conditions can then be expressed as (considering the normal $\vec{n}$ at the interface directed toward the vapor):

$$T(z=0) = T_w \tag{15}$$

$$h_i\left(T(r=R) - T_\infty\right) = -k_l \frac{\partial T}{\partial n} \tag{16}$$

Equations (14), (15) and (16) can be written in a non-dimensional form considering the following changes of variables:

$$r^* = \frac{r}{R}\ ;\ z^* = \frac{z}{R}\ ;\ \xi = \frac{T - T_w}{T_\infty - T_w} \tag{17}$$

We then obtain for the energy equation:

$$\frac{\partial^2 \xi}{\partial z^{*2}} + \frac{1}{r^*}\frac{\partial \xi}{\partial r^*} + \frac{\partial^2 \xi}{\partial r^{*2}} = 0 \tag{18}$$

And for the boundary conditions:

$$\xi_w = 0 \tag{19}$$

$$Bi\,(1-\xi) = \frac{\partial \xi}{\partial n^*} \tag{20}$$

where $Bi = \frac{h_i R}{k_l}$ is the Biot number.
To numerically solve the energy equation (18) along with boundary conditions (19) and (20), some precautions must be taken on the meshing as the heat flux may be concentrated on a very small region. This point is discussed in details in the following section.

2.1. Numerical considerations and data reduction

The system has to be solved for each dynamic contact angle that defines the drop geometry and for a large range of Biot number in order to generate a result database that covers all the potential applications. We used the Wolfram Mathematica Finite Element Method solver to solve the stationary axisymmetric non-dimensional Laplace equation (18). An adapted mesh was created for each case with a particular care taken to generate a mesh structured correctly to capture the temperature and heat flux fields (see Figure 1). The number of elements varies from about 50 000 up to 1 800 000 according to the contact angle and Biot number. We used second order elements (mainly triangles but also quadrilateral elements). The mesh quality (computed so that for regular polygons it is equal to 1 and for degenerate polygons is equal to zero) is set to "maximal" and the meshing routine will try for the best quality that can be achieved. We set the working precision to machine precision (24 digits), while the accuracy goal (absolute precision) was set to 16 digits. The "Pardiso" direct solver that is optimized for speed and memory efficiency has been used. A fully detailed description of the method, the solver, the implementation, as well as several validation cases can be found in [17]. To ensure a good quality of the solution, the heat flux conservation was systematically checked. A specific attention has been paid on the heat flux spatial distribution near the triple line and the mesh has been locally refined to this end.

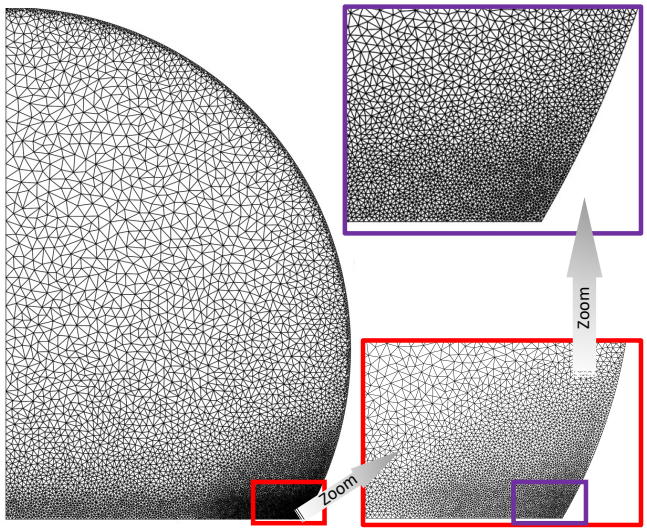

Figure 1: Example of a drop mesh for an dynamic angle of 120° ; the symmetry axis is the left one. It is an unstructured mesh composed of 281466 2^{nd} order triangle elements. The smallest element near the triple line has here a typical size of $10^{-4}R$ (this value is about $\frac{1}{Bi}$ for all the calculations).

The average interface temperature $\overline{\xi_i}$ was then calculated by simple integration of the local temperature on the interface. The total heat transfer rate Ψ across the (non-dimensional) drop

was then determined in three ways, i.e. by integration of the conduction heat flux along the wall, by integration of the conduction heat flux below the interface, and by integration of the convection heat flux above the interface:

$$\Psi = \int_{\alpha} -k_l \frac{\partial \xi}{\partial n^*} dS^* \text{ with } \alpha = \text{i or w} \tag{21}$$

$$= \int_{\text{i}} Bi\,(\xi_i - 1)\,dS^* = Bi\ S_i^*\ \left(\overline{\xi_i} - 1\right) \tag{22}$$

Considering Equation 22 for the non-dimensional heat transfer rate, the non-dimensional thermal resistance by conduction in the liquid is simply expressed as:

$$\mathcal{R}_{th} = \frac{\overline{\xi_i}}{\overline{\Psi}} \tag{23}$$

The dimensional thermal resistance (K/W) is easily deduced :

$$R_{th} = \frac{\mathcal{R}_{th}}{k_l R} \tag{24}$$

It is well known that finite element method converge toward the exact solution of conduction

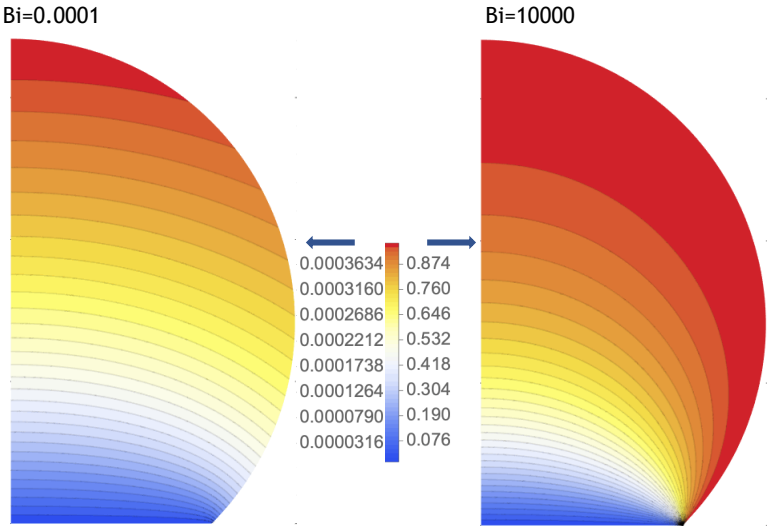

Figure 2: Examples of non-dimensional temperature field (ξ) calculated for a dynamic contact angle of 135° and two values of Biot number (10^{-4} and 10^4). As indicated by the isotherm shape, the heat flux is more concentrated near the triple line at high Biot number.

equation for a sufficient fine mesh. Also, the spatial domain should be discretized with a sufficient accuracy to avoid geometrical errors. We choose to use second order elements to mesh the sphere segment, thus even for relatively large element the interface shape will be captured. Examples of non-dimensional temperature field (ξ) are reported on Fig. 2 in the case of a dynamic contact angle $\theta = 135°$ and two different Biot numbers ($Bi = 10^{-4}$ and $Bi = 10^4$). The temperature fields appear quite different in the two configurations.

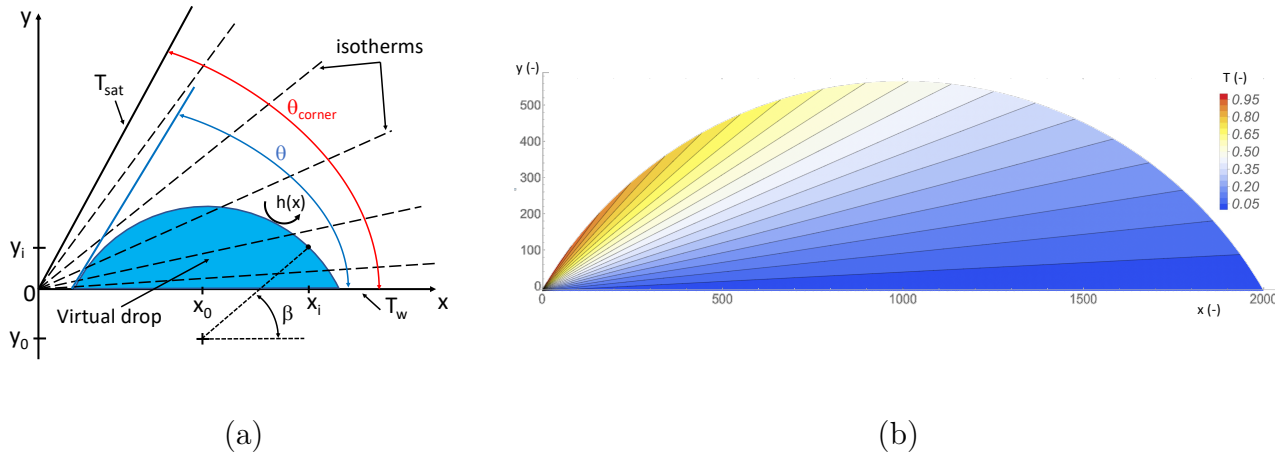

(a) (b)

Figure 3: Configuration of the reference case. The local heat flux in such a configuration can be determined analytically and is thus used to check the numerical results precision. b) Example of temperature field obtained with the finite elements tool when imposing $h(\beta)$ accordingly to Equation (26) with $x_0 = 0.972\,R\sin\theta$, $\theta = 60°$ and $\theta_{corner} = 63°$.

In order to construct a mesh that leads to precise enough data for the final aim of the simulation, the point is not only to evaluate the solution error (temperature, global heat transfer rate conservation) according to the element size but also to ensure the quality of the derived quantities that will be used in the analysis. Since the heat flux is localized mainly in the vicinity of the triple line, the temperature gradient is concentrated in an area whose size decreases sharply with increasing Biot. So, this extremely sharp spatial distribution of the heat flux, associated with the axisymmetric geometry of the drop, induces a significant difficulty in determining a size (or rather a field of sizes) of meshes suitable for guaranteeing the quality of the solution and particularly the exact calculation of the heat fluxes and heat transfer rate. We thus defined a reference case, solved it and obtained an explicit algebraic solution (see Appendix). It was used to derive a criterion on the mesh element size leading to an accurate solution. This reference case and the obtained mesh criterion are detailed in the following section.

2.2. Mesh element size criterion for accurate numerical solution

To define the reference case, let us consider first two isothermal planes at temperature T_{sat} and T_w, forming a corner of angle θ_{corner}. Due to symmetry considerations, the isotherms in this corner are straight lines passing through the origin (Figure 3.a):

$$T(x,y) = \frac{T_{sat} - T_w}{\theta_{corner}} \arctan\left(\frac{y}{x}\right) + T_w \tag{25}$$

Let us now consider a virtual 2D droplet of radius R and contact angle θ in this corner, the center of this virtual drop being placed at (x_0, y_0) from the origin of the corner. This virtual droplet has then its footprint at uniform temperature T_w and can be considered as exchanging heat with the plane at T_{sat} with an apparent heat transfer coefficient h which varies along the interface of the drop. So, h has to be determined locally so that the temperature field in

the drop is identical to the one in the corner. The resulting expression of h on the interface according to the angular position β around the drop center is (cf. Appendix):

$$h(\beta) = \frac{ak_l\left(x_0\frac{y_i}{x_i} - y_0\right)}{R\,x_i\left(1+\frac{y_i^2}{x_i^2}\right)\left(T_{sat} - T_w - a\arctan\left(\frac{y_i}{x_i}\right)\right)} \tag{26}$$

with :

$$a = \frac{T_{sat} - T_w}{\theta_{corner}} \tag{27}$$

and

$$x_i = R\cos\beta + x_0,\ y_i = R\sin\beta + y_0,\ y_0 = -Rcos\theta \tag{28}$$

Both local heat flux in the zone $x_0 - R\sin(\theta) \leq x \leq x_0 + R\sin(\theta)$ and heat transfer rate through the drop can be easily deduced:

$$q(x) = -\frac{ak_l}{x} \tag{29}$$

$$Q = a\ln\left(\frac{x_0 + R\sin(\theta)}{x_0 - R\sin(\theta)}\right) \tag{30}$$

The interesting point is that playing with the center abscissa x_0 and the angle θ_{corner} we can both obtain more or less sharp heat flux distribution and very high local values of the Biot number.

We reported in Table 1 the heat transfer rate calculated using finite element code as well as the one given by Equation (30). We chose x_0 so that $\frac{x_0 - R\sin\theta}{R}$ is in the range $[0.01; 10]$ leading to a maximum local Biot number (defined as $\frac{h(\beta)R}{k_l}$) in the left corner varying between $2\cdot10^2$ and $2\cdot10^5$, the latter corresponding to almost the worst case encountered in dropwise condensation. Calculations have been realized for both hydrophilic and hydrophobic situations, i.e., for $\theta = 60°$ ($\theta_{corner} = 63°$) and $\theta = 130°$ ($\theta_{corner} = 132°$). An example of the temperature field obtained with the finite elements code is reported on Figure 3.b in the case $\theta = 60°$. The isotherms obtained numerically are straight lines as expected, and are well superposed to the isotherms obtained analytically.

From general point of view, the meshing requirements are function of the geometry, the boundary conditions and the numerical method. To check the convergence, several meshes have been used, each of them being characterized by the size of the smallest element in the triple line vicinity. As it can be seen in Table 1, a good agreement between numerical results and analytical ones is obtained when the non-dimensional size of the element is less than the inverse of the local Biot number. This rule, even if it is specific to the present case, has been found to remain true whatever the values of x_0, θ_{corner} and θ. It is worth noting that such a dependence of the mesh element to the local Biot number is not surprising as the local heat flux is a function of the inverse of the local abscissa. So, to capture the right value of the heat flux, element size of the mesh has to vary accordingly.

It can be noticed that the chosen mesh requirement in literature fall in line with our proposed criterion. For example, in their mesh convergence analysis, Chavan et al. [14] (see S2 of their supplementary material) remarked that mesh size has to be smaller than R/100 for a Biot

θ	θ_{corner}	Bi_{max}	(Size of the smallest element)/R	$Q/(\lambda R \Delta T)$ FE	$Q/(\lambda R \Delta T)$ analytic	Relative deviation (%)
60°	63°	211.2	$2.70 \cdot 10^{-4}$	5.4467	5.4467	0.00
60°	63°	2135.6	$6.85 \cdot 10^{-5}$	7.54466	7.54285	0.02
60°	63°	23757.4	$3.37 \cdot 10^{-5}$	9.79803	9.73298	0.67
60°	63°	101827	$3.44 \cdot 10^{-5}$	11.1804	11.0565	1.12
60°	63°	213839	$3.65 \cdot 10^{-5}$	12.1979	11.7313	3.98
130°	132°	280.0	$2.27 \cdot 10^{-4}$	2.59957	2.59956	0.00
130°	132°	2866.5	$7.02 \cdot 10^{-5}$	3.60461	3.60000	0.13
130°	132°	31931.3	$1.10 \cdot 10^{-5}$	4.64803	4.64529	0.06
130°	132°	136875	$6.83 \cdot 10^{-6}$	5.17683	5.27697	-1.90
130°	132°	287446	$7.03 \cdot 10^{-6}$	5.77299	5.59902	3.11

Table 1: Non-dimensional heat transfer rate through the 2D droplet obtained with the finite elements (FE) code and with Equation 30 for 2 dynamic contact angles (60° and 130°). The reported Biot number is the maximum local value of $\frac{h(\beta)R}{k_l}$ with $h(\beta)$ calculated using Equation 26.

number of 100 in order to achieve mesh convergence. Although these studies were carried out following the best practice in the domain (mesh convergence analysis, comparison with available data, convergence criteria ....), the tests were carried out for an average representative Biot number (an usual procedure efficient for the majority of problems) and not for the maximal one. The specific spatial distribution of the interfacial heat transfer rate that becomes more and more localized and peaked with increasing Bi induced inaccuracies in the produced results. Indeed, when the element size is too big compared to the peak width, a significant part of the total heat transfer is missed without any clear indication on the convergence criteria. The difference between two consecutive meshes can thus be small while both values are far from the exact solution. In other words, the calculated heat transfer rate can remain appreciably constant on a rather large range of mesh size without being completely converged.

It thus appears that determining precise solutions (heat transfer and temperature on the interface) is more complicated than what one might suppose based on an usual good practice in numerical modeling. We also performed several preliminary tests with finite volume and finite element methods using commercial software to facilitate pre- and post-processing (Wolfram Mathematica and Siemens Starccm+) and compared the obtained results. As expected, we observed excellent agreement between all codes for low and moderate Biot values. Using *sufficiently refined* meshes (depending on the method and the used software), similar data were produced using all methods even for high Biot ; however we also have observed that in some cases all the codes gave similar results for a given refinement level but finally converged to a different solution upon further refinement.

We decided to carry out the systematic study using the finite element method in the Mathematica environment, developed a specific mesh strategy and, set up a calculation module to obtain reference data and to confirm the precision of our solutions.

So, the developed meshing algorithm uses a size function that defines a local element size (either a length or an area) as a function of the coordinates of the element center, enforces an "accuracy goal constraint" on the node placement along the boundaries and simultaneously maximizes the mesh quality. The resulting mesh structure is as follow (see figure 1) : the smallest element size

near the triple line is about $\frac{1}{Bi}$, and grows roughly inversely with the distance to this point. In addition, a layer of fine meshes is created in the vicinity of the interface for heat flux accuracy calculation and post-processing purposes.
Consequently, to validate the accuracy of the solution on this tricky problem and when using such a meshing algorithm, an *adhoc* code has been developed using a completely different numerical approach (i.e. Monte Carlo) in order to produce a reference set of data. This code is detailed in the next section.

2.3. Confrontation with an independent tool based on Monte Carlo method

Statistical methods for solving the diffusion equation were initiated in the 1950s from the concomitant development of Monte Carlo methods and the work of Feynmann and Kac who established the link between parabolic partial differential equations and stochastic processes [18, 19]. The idea is to define the quantity of interest (here the temperature) as the expectation of random processes, which is numerically evaluated by an average over samples of random walk paths. The result becomes closer to the expected value as the number of samples is increased [20, 21, 22].
Walk on Sphere (WoS) methods [23, 24, 25] are directly part of this story, but in the simpler case where the diffusion equation is stationary and homogeneous (Laplace equation), it is possible to directly build the algorithmic idea from the properties of harmonic functions. This property states that the temperature at any point is equal to the average of the temperatures on any sphere included in the domain and centered around the point.
Adding the idea of double randomization (central concept in Monte Carlo methods) [26], allows the construction of random walk paths by successively sampling positions on spheres of any radius. Typically, in our case, to evaluate the temperature at a given point, we construct a large sample of paths (each of them is a succession of segments of different sizes and directions) that start from this point and end on boundaries where the temperature is known. The average of the temperatures obtained at the end of the paths is an unbiased estimator of the desired temperature. Recently, various works have extended the field of application to coupled heat transfers in complex geometry due to both theoretical advances on physical formulations and considerable computing progress on ray tracing capabilities from the image synthesis community [27, 28, 29].
In the present work we use the classical WoS method which consists in always choosing the largest sphere entirely included in the domain (its radius is the smallest distance to the boundary). The boundary is reached when the location sampled on the sphere is at a distance lower than a numerical parameter ϵ. An important property of this method is that the number of successive spheres required to reach the boundary increases only as the logarithm of $\frac{1}{\epsilon}$ [30]. Thus it is possible to choose values of ϵ close to the precision of computer representation of floating point numbers, which results in introducing almost no approximation due to this parameter (the ratio of epsilon to the characteristic dimension of the domain is in our case always lower than 10^{-8}).
In our configuration, if the random walk reaches the foot of the drop, the dimensionless temperature given by equation 19 is retained (here 0). On the other hand, the boundary condition at the liquid-vapor interface given by equation 20 requires a particular treatment which introduces a new numerical parameter. Approximating normal derivative of the equation 20 by a finite difference, it is straightforward to write the non-dimensional temperature at the interface as an

expectation:

$$\xi_I = P\,\xi_\infty + (1-P)\,\xi_{\delta_I}$$

where $\xi_\infty = 1$, $P = \frac{Bi\,\delta_I}{Bi\,\delta_I+1}$ and ξ_{δ_I} is the temperature of the point on the normal line at a distance δ_I from the interface. Thus, when the path reaches the liquid-vapor interface, with probability P it ends in the vapor and the weight is the corresponding dimensionless temperature (here 1), and with probability (1-P) the path continues in the drop from the reinjection position (defined by the numerical parameter δ_I).

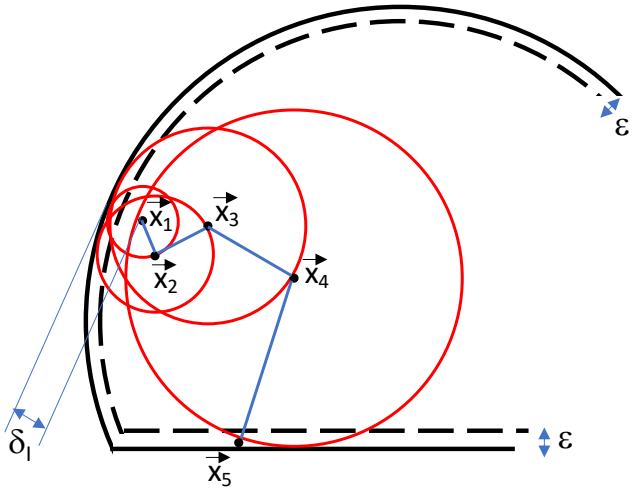

Figure 4: Walk on Sphere Illustration. A random walk path connecting the centers of the spheres $\vec{x}_i$ is represented by a blue line. After a reinjection the point $\vec{x}_1$ is at a distance δ_I from the liquid-vapor interface and the last point of the path $\vec{x}_5$ is at a distance from the wall smaller than ϵ.

The numerical re-injection parameter δ_I must be as small as possible to ensure that the temperature gradient at the interface is well represented. This is especially important near the triple line with high Biot values, as the gradient can then be huge. As a consequence, when the re-injection takes place near the triple line region, the re-injection parameter is gradually decreased towards ϵ in an empirical way. Additionally, if the distance of the foot of the drop is lower than $2 \times \epsilon$, the parameter is set to the exact distance of the foot of the drop (so that the re-injection reaches it). All the simulations are done after having checked that the influence of this parameter on the results is no longer perceptible (δ_I is then typically $100 \times \epsilon$).

The calculation of the flux given by equation 22, simply requires an additional integration in Monte Carlo to evaluate the average temperature on the liquid vapor interface. Since the flux is mostly concentrated around the triple line for large values of the Biot number, it could be interesting, for a further evolution of the method, to set up a sampling strategy to decrease the variance of the estimator (which will directly decrease the computation time).

The software used for the Monte Carlo computations, namely "Droplet", is available online as a git repository [31] and is distributed under the GPLv3+ license. It is a C program which is based on the Star-Engine, a free development environment that is developed by Méso-Star [32] and whose main purpose is to help engineers and researchers to develop Monte Carlo

simulation software. Star-Engine is made of several libraries, each one focused on a single functionality following an Unix-inspired philosophy (random numbers generation, 2D and 3D complex geometry ray-tracing and sampling, mesh I/O, mesh generation, scattering functions, volume ray-tracing, unstructured volume data management, ...). The Star-Engine can be freely downloaded [33].

		Monte Carlo			Finite elements
θ	Bi	$\Psi_{min} - \Psi_{max}$ (confidence of 99.7%)	Median value	Number of samples	Ψ
20°	0.0001	$3.789 \cdot 10^{-5} - 3.789 \cdot 10^{-5}$	$3.789 \cdot 10^{-5}$	10^5	$3.789 \cdot 10^{-5}$
20°	0.1024	$0.03865 - 0.03869$	0.03867	10^5	0.03868
20°	104.86	$12.314 - 12.363$	12.339	$5 \cdot 10^6$	12.334
20°	107374	$53.956 - 54.0821$	54.0191	$5 \cdot 10^9$	54.071
70°	0.0001	$4.133 \cdot 10^{-4} - 4.135 \cdot 10^{-4}$	$4.134 \cdot 10^{-4}$	10^4	$4.134 \cdot 10^{-4}$
70°	0.1024	$0.4052 - 0.4075$	0.4064	$5 \cdot 10^6$	0.4056
70°	104.86	$20.843 - 21.025$	20.934	10^7	20.959
70°	107374	$53.970 - 54.2635$	54.117	10^{10}	54.233
120°	0.0001	$9.415 \cdot 10^{-4} - 9.427 \cdot 10^{-4}$	$9.421 \cdot 10^{-4}$	10^4	$9.423 \cdot 10^{-4}$
120°	0.1024	$0.8078 - 0.8145$	0.81115	10^5	0.8106
120°	104.86	$13.314 - 13.531$	13.4225	10^7	13.455
120°	107374	$30.802 - 31.138$	30.97	10^{10}	31.115
170°	0.0001	$1.244 \cdot 10^{-3} - 1.245 \cdot 10^{-3}$	$1.2445 \cdot 10^{-3}$	10^4	$1.244 \cdot 10^{-3}$
170°	0.1024	$0.4482 - 0.4598$	0.454	10^5	0.4523
170°	104.86	$1.6728 - 1.7361$	1.70445	$2 \cdot 10^7$	1.699
170°	107374	$4.006 - 4.146$	4.076	10^{10}	4.074

Table 2: Non-dimensional heat transfer rate obtained with the finite elements code and with the Monte-Carlo method for 4 dynamic contact angles (20°, 70°, 120° and 170°) and 4 Biot numbers $10^{-4}\times$ (1, 2^{10}, 2^{20} and 2^{30}). The number of samples for MC computations is chosen as a compromise between standard deviation, which decreases as the square root of the number of samples, and computation time. Compatibility between the two approaches is systematically satisfied.

In its current version, the "Droplet" software main characteristics are:

- It is dedicated to the droplet problem discussed in this paper and has been carefully validated against the reference case "corner" described on figure 3 for which exact solution is available. In all the tested configurations representative of the Biot numbers of the problem (locally up to $2 \cdot 10^5$) we calculated the temperature on several points on the interface as well as the global heat flux (surface probe). The number of samples was adjusted until the relative standard deviation $\frac{\sigma}{\chi}$ on the estimate value χ was less than 0.1%. The exact value χ_{exact} (eq. 25 for the temperature or eq. 30 for the heat flux) is then found in the range $\pm 3\sigma$ around the estimate value χ.

- Geometric computations are analytic (not approximated with a mesh) and all computations are carried out in double precision,

- "Droplet" is a command-line tool and its parameters can be modified through dedicated command-line options.

As illustrated by table 2, the two numerical approaches are in excellent agreement. This hereby confirms the validity of the numerical results and allows us to confidently use the data set to generate an accurate correlation in order to predict the droplet heat transfer in various conditions. At low Biot, the heat transfer rate increases with contact angle -i.e., the interface area- as the heat flux is roughly homogeneous in the droplet while at high Biot it decreases (on the presented range) as it is mostly proportional to the triple line length.

3. Correlation for the conduction thermal resistance of the drop

The thermal resistance of the droplet was deduced from the interface average temperature (calculated by integration of the local temperature, see Eq. 22) and the total heat transfer across the droplet. To produce accurate data, the procedure described above regarding the meshing and the convergence criteria was carried out for 61 contact angles ranging linearly from 20° up to 170° and for 31 Biot numbers distributed exponentially from 10^{-4} up to 10^{5} in order to spread the 1891 data points over a range exceeding the physically accessible one. The contact angle range covers the whole possible situations from hydrophylic cases to hydrophobic ones. The Biot range corresponds to water droplets radii up to few millimeters at atmospheric pressure (i.e. when the condensation coefficient is set to 1 when calculating h_i). For illustration purpose, we reported in Table 3 the drop curvature radius and the heat transfer coefficient values in the case of water at atmospheric pressure for different Biot numbers. If the condensation coefficient f is set to 1 (corresponding to the maximal value of $h_i = 15.7 \cdot 10^6\ Wm^{-2}K^{-1}$), for Bi in the range 10^{-4} the curvature radius of the drop would be non-physically small. Similarly, for a $1nm$ radius drop, values of Bi above 0.25 could not be obtained as it would implies a heat transfer coefficient greater than the maximal physical value.

The variations of the dimensionless conduction thermal resistance ratio $\mathcal{R}_{th}/\mathcal{R}_{th,0}$ obtained

	R (m) for two h_i $(W.m^{-2}.K^{-1})$		h_i $(W.m^{-2}.K^{-1})$ for two R (m)	
Biot	$h_i = 15.7 \cdot 10^6$ (f=1)	$h_i = 4.03 \cdot 10^5$ (f=0.05)	R=10^{-9}	R=10^{-3}
0.0001		$1.54 \cdot 10^{-10}$	$6.2 \cdot 10^3$	$6.2 \cdot 10^{-2}$
0.1	$3.95 \cdot 10^{-9}$	$1.54 \cdot 10^{-7}$	$6.2 \cdot 10^6$	$6.2 \cdot 10^1$
100	$3.95 \cdot 10^{-6}$	$1.54 \cdot 10^{-4}$		$6.2 \cdot 10^4$
100000	$3.95 \cdot 10^{-3}$	0.154		

Table 3: Considering water as a working fluid $k_l \approx 0.62\ Wm^{-1}K^{-1}$ varying Bi from 10^{-4} up to 10^{5} is obtained by varying the product $h_i R$. The greyed cells correspond to non-physically obtainable values.

from numerical data are reported on Figure 5 as a function of $\log_{10}(Bi)$. For each dynamic contact angle θ, $\mathcal{R}_{th,0}$ is the dimensionless thermal resistance for the lowest Bi value -i.e., for $Bi = 10^{-4}$-. Each curve corresponds to a single dynamic contact angle ; the resistance ratio decreases with contact angle up to about 145° and then increases significantly. This trend is mostly apparent for $1 < Bi < 10^4$; outside of this range the variations versus contact angle are very small. It can be noticed from this figure that $\mathcal{R}_{th}/\mathcal{R}_{th,0}$ remains almost constant and equal to 1 when Bi is smaller than 10^{-2} whatever the contact angle. This behavior can be

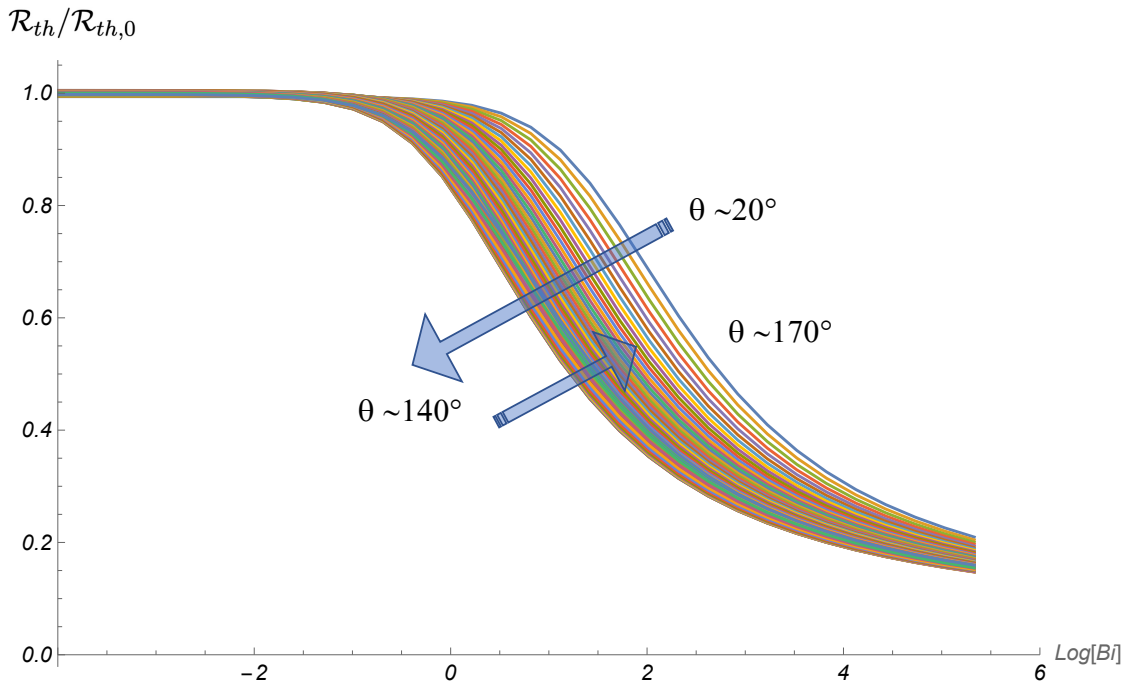

Figure 5: Reduced thermal resistance versus $\log_{10}(Bi)$ for all tested dynamic contact angles : all the curves present a similar sigmoidal step shape

explained as follows: when Bi is small, the conduction thermal resistance is small compared to the interfacial resistance. So, the heat transfer rate is mainly controlled by the convective effects, and the Biot number value has no more influence. For higher values of Bi, i.e., for Bi varying from 10^{-2} to 10^{5}, $\mathcal{R}_{th}/\mathcal{R}_{th,0}$ decreases in a nearly sigmoidal manner. As Bi increases, conduction thermal resistance becomes more and more predominant. The heat flux is then increasingly concentrated in the triple line region and the heat transfer rate becomes strongly correlated to the triple line length.

As all curves present the same shape, we propose to fit them by a simple sum of hyperbolic tangent functions of Biot in which the 5 parameters (ζ_i) depend only on the contact angle. The best fit for each contact angle was obtained using the Mathematica nonlinear fit algorithm along with the ζ_i expressions:

- For $Bi \leq 10^{-2}$

$$R_{th} = \frac{\zeta_0 \zeta_4}{kR} \tag{31}$$

- For $10^{-2} < Bi < 10^{5}$

$$R_{th} = \frac{\zeta_0}{kR} \left[\tanh\left\{\zeta_1 - \log_{10}(Bi)\right\} - \tanh\left\{\zeta_2 + \zeta_3 \log_{10}(Bi)\right\} + \zeta_4\right] \tag{32}$$

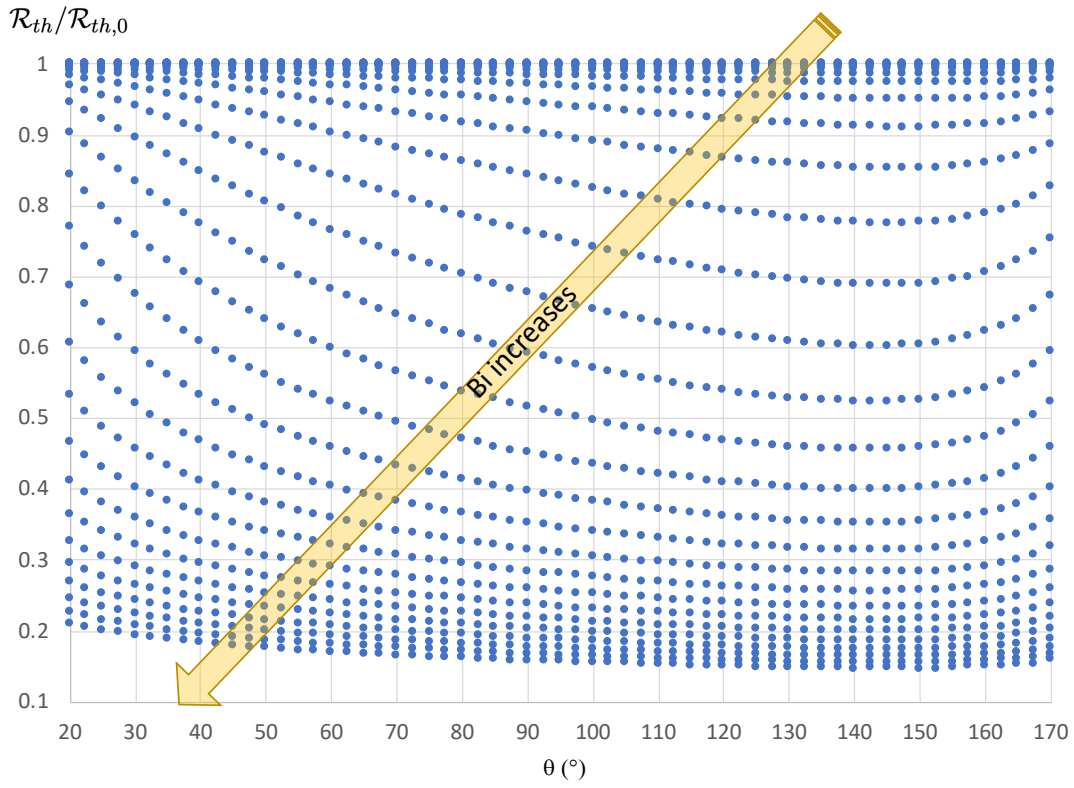

Figure 6: Reduced thermal resistance versus dynamic contact angle for all tested Biot numbers : all the curves present a similar more or less pronounced asymetric "U" shape ; the minimum is close to 145°.

where $\zeta_0 ... \zeta_4$ are function of θ expressed as a :

$$\zeta_i = \sum_{j=0}^{6} a_{ij}\theta^j + b_i \tan\left(\frac{\theta}{2}\right) \tag{33}$$

The values of constants a_{ij} and b_i are reported in Table 4. Examples of the variations of the dimensionless thermal resistances $\mathcal{R}_{th}$ obtained using this correlation as a function of the Bi number are reported on Figure 7 for 4 different contact angles. The symbols correspond to the numerical calculations. The adequacy appears very good whatever the Bi number and the contact angle. The comparisons between results obtained with Equations 31-33 and numerical data are reported on Figure 8 for all the considered configurations. As it can be seen on this figure, all data agree within ±4%. For most of the points the agreement is within about 1%. The highest discrepancy is obtained for the lowest values of the thermal resistance, thus for the highest Biot numbers and contact angles, where it reaches 4%. This was expected as it corresponds to the cases for which the heat flux is the most concentrated in the triple line vicinity.

As described in the introduction, 3 correlations from the literature are mainly used. They present different validity domains in terms of Biot numbers and contact angle ranges. For

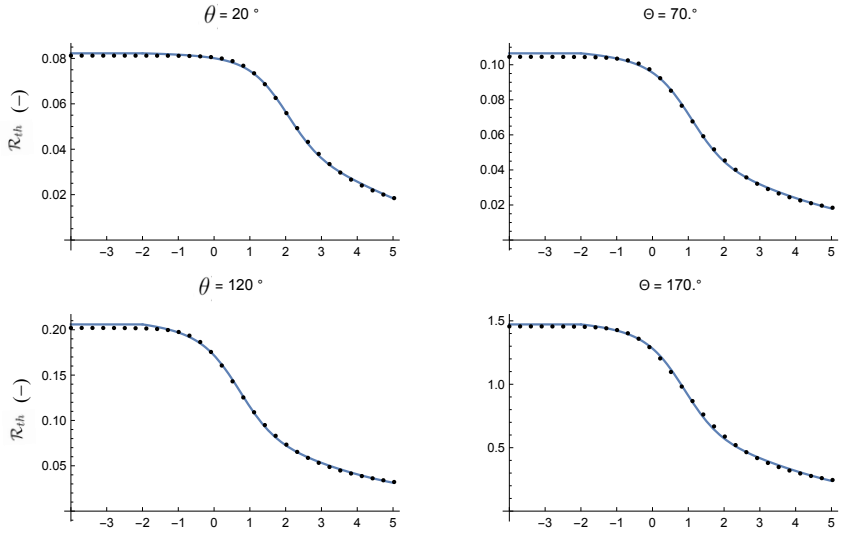

Figure 7: Non dimensional thermal resistance : Illustration of the good agreement between correlation values (lines) and original data (dots) for 4 dynamic contact angles.

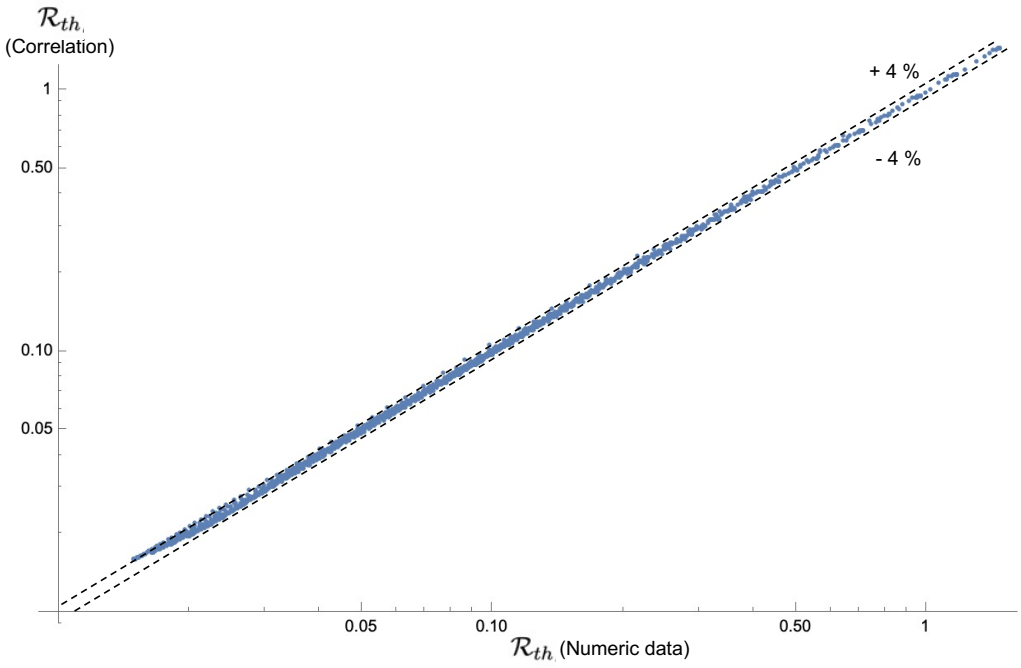

Figure 8: Non-dimensional thermal resistance (see eq. 23) : correlation values as a function of numerical ones for dynamic contact angle varying from 20° up to 170° and Biot numbers ranging from 10^{-4} up to 10^5 ; all the 1891 points lies in the range ±4% and the average difference is about 1.5%.

$\zeta_i \rightarrow$	ζ_0	ζ_1	ζ_2	ζ_3	ζ_4
a_{i0}	0.019944575	2.87624	-2.19022	0.414464	2.1726808
a_{i1}	-0.015866575	-3.00749	2.65388	-0.35213	-0.950956
a_{i2}	0.00149794	1.89873	-1.96457	0.322101	2.414324
a_{i3}	0	-0.645073	0.735545	-0.0938014	-2.231196
a_{i4}	0	0.087902	-0.107307	-0.031516	0.983096
a_{i5}	0	0	0	0.0237513	-0.2044184
a_{i6}	0	0	0	-0.00367889	0.01565884
b_i	0.03313825	0.0215536	0	0	0

Table 4: Values of constants a_{ij} and b_i in Equation (33).

example, Chavan et al. [14] law is only valid for hydrophobic situations, Kim and Kim [16] model is independent of Biot numbers and Adhikari et al. [15] correlation is proposed only for $Bi < 10^3$. In the following comparison, we will nevertheless plot the literature correlations over the full range used in the present study for comparison purpose and we will use dashed line when the curves are plotted outside of the validity range defined by the authors. Note as already explained that Chavan et al. as well as Adhikari et al. works report only the global thermal resistance -i.e. the sum of the one due to the conduction in the liquid and the interfacial one- and that we extract the droplet conduction resistance from their data. We thus conduct the comparison both in terms of global and conduction thermal resistances.

Figures 9.a and 9.b illustrate the deviation of the literature correlations to the present work for an hydrophilic situation. The first remark is that one could observe very important discrepancies. Secondly each these laws are usable only to some limited cases (either in terms of Bi or of dynamic contact angles). As expected, the Chavan law is clearly not applicable because the extrapolation of Equations 9-11 is not valid for contact angles smaller than 90°. On Figure 9.a Kim and Kim and Adhikari et al. global thermal resistances fairly agree with our data for Biot number up to one and remain applicable for Biot numbers smaller than 10 and 1000 respectively. For higher values of Biot number the discrepancies increase sharply. This is due to the imprecise estimation of the conduction thermal resistance as illustrated on Figure 9.b. As previously mentioned the insufficient meshing in Adhikari et al. work leads to a wrong estimation of the heat flux and thus induces an important bias on thermal resistance at high Biot numbers. For $Bi < 1$ the conduction resistance is negligible compared to the global one and thus extracting it from the global resistance is hazardous. This can explain the huge discrepancies observed. For hydrophilic situation the Adhikari law does not produce accurate results also for intermediate Biot numbers, while it gives rather good results at 90° and usable ones for hydrophobic situations (figures 9.d and f).
The model of Kim and Kim predicts accurately the conduction resistance for the small Biot numbers while it is clearly not applicable for $Bi > 10$ for all contact angles. This is probably due to the respective validity of the 2 main assumptions of this model: the interface is an isotherm, and the distance between 2 consecutive isotherms is half the distance on the symmetry axis.
Similar comments can be derived for intermediate contact angle i.e. (90 °, see Figure 9.c and 9.d) and high contact angle (135° see Figures 9.e and 9.f). For $\theta = 90°$, Adhikari et al. obtain accurate results for both the global and conduction thermal resistances up to $Bi = 1000$. This was as expected as this contact angle is taken as reference in the definition of their scaling

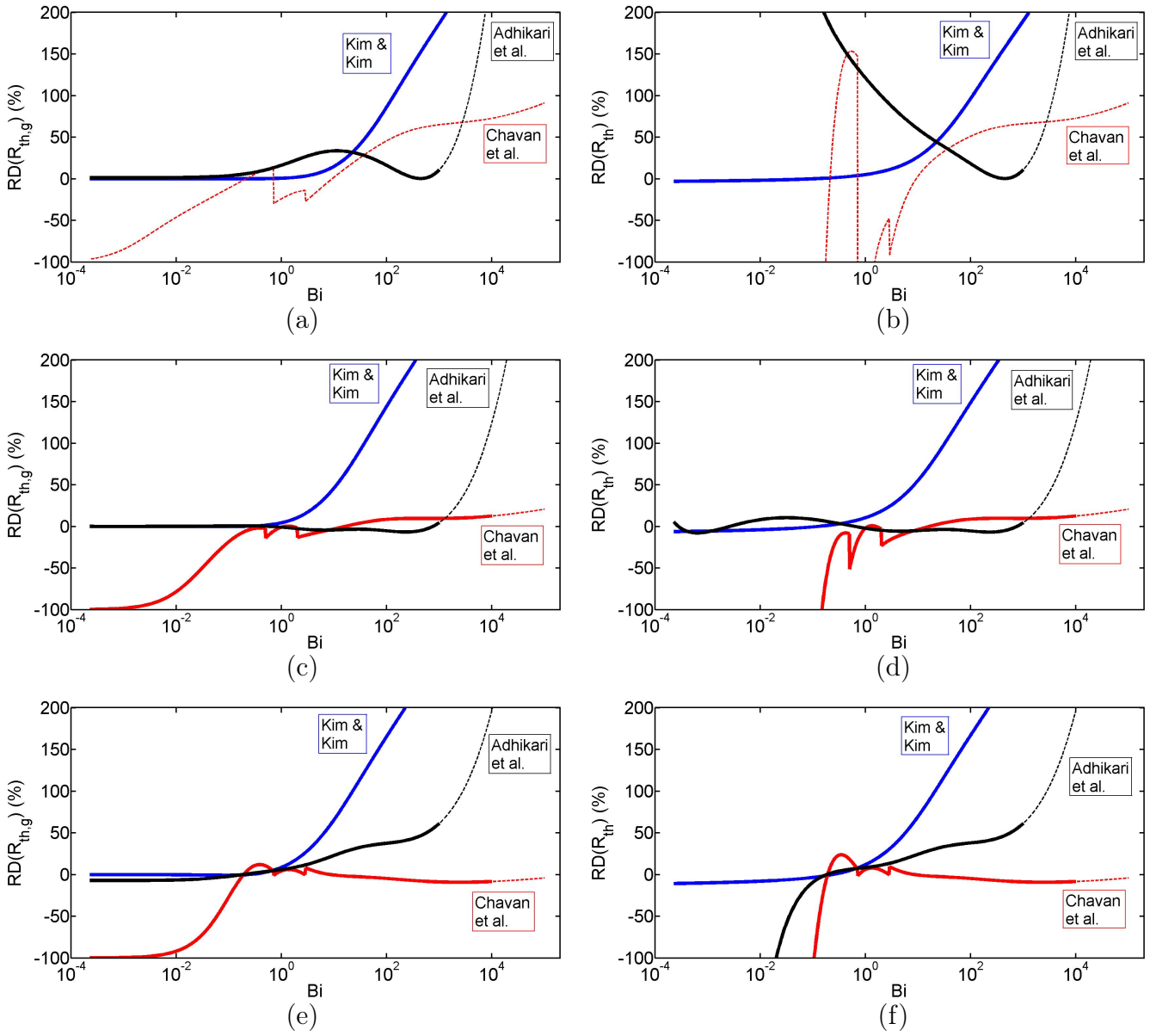

Figure 9: Relative deviation of the literature correlations to the present work for both global (i.e., liquid + interfacial) (left) and liquid (right) thermal resistances: (a and b) $\theta = 45°$; (c and d) $\theta = 90°$; (e and f) $\theta = 135°$. Thin dashed lines indicate that the correlation has been used outside of the validity range announced by the authors. Blue curves Kim and Kim [16], Red curves Chavan et al. [14], Black curves Adhikari et al. [15]. The Chavan et al. and Adhikari et al. liquid thermal resistances have been calculated as the difference between the global one and the interfacial one using respectively equations 8 and 12 along with equation 6 to evaluate the heat transfer coefficient.

factor (see Equation 13). For $\theta = 135°$, Chavan et al. works give acceptable results for both resistances when $Bi > 0.1$ while for smaller Bi values the discrepancies diverge. To summarize, literature correlations can be used for the evaluation of the conduction thermal resistance for the following cases:

- Kim and Kim : only for $Bi \leq 1$
- Chavan et al. : $Bi \geq 0.1$ and $\theta \geq 90°$
- Adhikari et al. : $0.1 < Bi < 1000$ and $\theta \geq 90°$

While all work correctly on a limited range none of them could be used in a generic manner. The correlation proposed in this work appears thus useful for modelling dropwise condensation whatever the configuration.

4. Conclusion

The problem of the heat transfer through a sessile droplet on an isothermal substrate may appear simple. However, from numerical point of view when using finite elements code, it involves drastic problem of precision as the heat flux is concentrated on a very small region near the triple line. By considering a reference case whose exact analytical solution is known and by comparing the results with an independent tool based on Monte Carlo method, it has been shown that the size of the mesh elements in the region of the triple line must be less than the inverse of the local Biot number in order to obtain good precision. Using this criterion, calculations of the conduction thermal resistance in the liquid has been done for dynamic contact angles varying from 20° to 170° and Biot number in the range $10^{-4} - 10^{5}$. An analytical regression law has then been derived that fits the numerical results with a maximum deviation of $\pm 4\%$ and an average one of about $\pm 1.5\%$. This law can thus be used with confidence when modeling dropwise condensation on hydrophilic, hydrophobic or heterogeneous wettability surface. Finally, comparisons with similar laws available in literature have been done. According to the configuration, i.e., contact angle and Biot number values, important discrepancies have been highlighted.

Acknowledgements

This work was funded by the European Space Agency, MAP ENCOM contract n°4200020276.

Appendix A. 2D heat transfer reference case "Corner"

To define our 2D reference case, let us consider first two isothermal planes at temperature T_{sat} and T_w, forming a corner of angle θ_{corner}. Due to symmetry considerations, the isotherms in this corner are straight lines passing through the origin (Figure 3.a):

$$T(x, y) = a \arctan\left(\frac{y}{x}\right) + T_w \tag{A.1}$$

with:

$$a = \frac{T_{sat} - T_w}{\theta_{corner}} \tag{A.2}$$

The temperature gradient is thus obtained by simple derivation:

$$\vec{grad}(T) = \frac{a}{x(1+\frac{y^2}{x^2})}\left(-\frac{y}{x}\vec{e}_x + \vec{e}_y\right) \tag{A.3}$$

The resulting expression of the coordinates of any point on the interface i according to the angular position β around the drop center is:

$$x_i = R\cos\beta + x_0,\ y_i = R\sin\beta + y_0 \tag{A.4}$$

The normal to the liquid-vapor interface is:

$$\vec{n}_i = \frac{x_i - x_0}{R}\vec{e}_x + \frac{y_i - y_0}{R}\vec{e}_y \tag{A.5}$$

So, the conduction heat flux at the interface can be expressed as:

$$q = -k_l\ \left(\vec{grad}(T).\vec{n}\right)_i = -\frac{ak_l\left(x_0\frac{y_i}{x_i} - y_0\right)}{R\,x_i\left(1+\frac{y_i^2}{x_i^2}\right)} \tag{A.6}$$

This heat flux can also be expressed using Newton's law:

$$q = -h(\beta)(T_{sat} - T_i) = -h(\beta)\left(T_{sat} - T_w - a\arctan\left(\frac{y_i}{x_i}\right)\right) \tag{A.7}$$

The local heat transfer coefficient $h(\beta)$ is thus finally:

$$h(\beta) = \frac{ak_l\left(x_0\frac{y_i}{x_i} - y_0\right)}{R\,x_i\left(1+\frac{y_i^2}{x_i^2}\right)\left(T_{sat} - T_w - a\arctan\left(\frac{y_i}{x_i}\right)\right)} \tag{A.8}$$

References

[1] F. Kreith and R.F. Bohem. *Direct-Contact Heat Transfer*. Springer-Verlag, Berlin, Heidelberg GmbH, 1953.

[2] E. Schmidt, W. Schurig, and W. Sellschopp. Versuche über die kondensation von wasserdampf in film- und tropfenform. *Technische Mechanik und Thermodynamik*, 1(2):53–63, 1930.

[3] M. Singh, N.D. Pawar, S. Kondaraju, and S.S. Bahga. Modeling and simulation of dropwise condensation: a review. *Journal of the Indian Institute of Science*, 99(1):157–171, 2019.

[4] B. El Fil, G. Kini, and S. Garimella. A review of dropwise condensation: Theory, modeling, experiments, and applications. *International Journal of Heat and Mass Transfer*, 160:120–172, 2020.

[5] S.H. Zheng, U. Gross, and X.D. Wang. Dropwise condensation from fundamentals of wetting, nucleation, and droplet mobility to performance improvement by advanced functional surfaces. *Advances in Colloid and Interface Science*, 295:102503, 2021.

[6] A. Goswami, S.C. Pillai, and G. McGranaghan. Surface modifications to enhance dropwise condensation. *Surfaces and Interfaces*, 25:101143, 2021.

[7] J. Lethuillier, P. Lavieille, and M. Miscevic. About the role of falling droplets' sweeping in surface renewal during dropwise condensation. *Langmuir*, 36(43):12877–12886, 2020.

[8] H.W. Wen and R.M. Jer. On the heat transfer in dropwise condensation. *The Chemical Engineering Journal*, 12(3):225–231, 1976.

[9] S. Zheng, F. Eimann, C. Philipp, T. Fieback, and U. Gross. Modeling of heat and mass transfer for dropwise condensation of moist air and the experimental validation. *International Journal of Heat and Mass Transfer*, 120:879–894, 2018.

[10] M. Mei, F. Hu, C. Han, and Y. Cheng. Time-averaged droplet size distribution in steady-state dropwise condensation. *International Journal of Heat and Mass Transfer*, 88:338–345, 2015.

[11] E.J. Le Fevre and J.W. Rose. A theory of heat transfer by dropwise condensation. *Proceeding of International Heat Transfer Conference*, 3, 1966.

[12] R.W. Schrage. *A Theoretical Study of Interphase Mass Transfer*. Columbia University Press, 1953.

[13] Van P Carey. *Liquid-vapor phase-change phenomena: an introduction to the thermophysics of vaporization and condensation processes in heat transfer equipment*. CRC Press, 2008.

[14] S. Chavan, H. Cha, D. Orejon, K. Nawaz, N. Singla, Y. F. Yeung, D. Park, D. H. Kang, Y. Chang, Y. Takata, and N. Miljkovic. Heat transfer through a condensate droplet on hydrophobic and nanostructured superhydrophobic surfaces. *Langmuir*, 32:7774–7787, 2016.

[15] S. Adhikari, M. Nabil, and A. S. Rattner. Condensation heat transfer in a sessile droplet at varying biot number and contact angle. *International Journal of Heat and Mass Transfer*, 115:926–931, 2017.

[16] S. Kim and K. J. Kim. Dropwise condensation modeling suitable for superhydrophobic surfaces. *Journal of Heat Transfer, trans ASME*, 133(8):081502, 2011.

[17] Wolfram mathematica. Wolfram fem guide. `https://reference.wolfram.com/language/FEMDocumentation/guide/FiniteElementMethodGuide.html`.

[18] M. Kac. On some connections between probability theory and differential and integral equations. In *Proceedings of the second Berkeley symposium on mathematical statistics and probability*. The Regents of the University of California, 1951.

[19] Pierre Del Moral. Feynman-kac formulae. In *Feynman-Kac Formulae: Genealogical and Interacting Particle Systems With Applications*. Springer, 2004.

[20] M.E. Muller et al. Some continuous monte carlo methods for the dirichlet problem. *The Annals of Mathematical Statistics*, 27(3):569–589, 1956.

[21] M. Grigoriu. A monte carlo solution of heat conduction and poisson equations. *Journal of Heat Transfer*, 122(1):40–45, 2000.

[22] C. Graham and D. Talay. *Stochastic simulation and Monte Carlo methods: mathematical foundations of stochastic simulation*, volume 68. Springer Science & Business Media, 2013.

[23] A. Haji-Sheikh and E.M. Sparrow. The floating random walk and its application to monte carlo solutions of heat equations. *SIAM Journal on Applied Mathematics*, 14(2):370–389, 1966.

[24] N.H Bingham. Random walk on spheres. *Zeitschrift für Wahrscheinlichkeitstheorie und Verwandte Gebiete*, 22(3):169–192, 1972.

[25] S. Hoshino and K. Ichida. Solution of partial differential equations by a modified random walk. *Numerische Mathematik*, 18(1):61–72, 1971.

[26] S. Maire and G. Nguyen. Stochastic finite differences for elliptic diffusion equations in stratified domains. *Mathematics and Computers in Simulation*, 121:146–165, 2016.

[27] R. Fournier, S. Blanco, V. Eymet, M. El Hafi, and C. Spiesser. Radiative, conductive and convective heat-transfers in a single monte carlo algorithm. In *Journal of Physics: Conference Series*, volume 676(1), pages art–012007, 2016.

[28] L. Ibarrart, C. Caliot, M. El Hafi, R. Fournier, S. Blanco, S. Dutour, J. Dauchet, J.M. Tregan, V. Eymet, and V. Forest. Combined conductive-convective-radiative heat transfer in complex geometry using the monte carlo method: Application to solar receivers. In *International Heat Transfer Conference Digital Library*. Begel House Inc., 2018.

[29] L. Penazzi, S. Blanco, C. Caliot, C. Coustet, M. El Hafi, R. Fournier, M. Galtier, L. Ibarrart, and M. Roger. Toward the use of symbolic monte carlo for conduction-radiation coupling in complex geometries. In *Proceedings of the 9th International Symposium on Radiative Transfer, RAD-19*. Begel House Inc., 2019.

[30] I. Binder and M. Braverman. The rate of convergence of the walk on spheres algorithm. *Geometric and Functional Analysis*, 22(3):558–587, 2012.

[31] Mesostar. Droplet, 2021. `https://gitlab.com/meso-star/droplet`.

[32] url of the company. `https://{www.meso-star.com}`.

[33] star engine url. `https://www.meso-star.com/projects/star-engine/star-engine.html`.